LED-based PIV of a particle-laden turbulent free surface

A. Anand[1,*], C. Poelma[1], A. Laskari[1]

1: Multiphase Systems, Process & Energy, Delft University of Technology, The Netherlands
*Corresponding author: a.anand-1@tudelft.nl

Keywords: Turbulence, Multiphase flows, Free-surface, PIV, PTV.

ABSTRACT

An experimental method is proposed to study dispersed two-phase flows at an air-water interface, a family of flows of practical significance in environmental and industrial settings. The applicability of this technique is demonstrated through the study of a lightly-deformed turbulent free-surface laden with floating particles ('floaters'). A low-mean turbulent flow is generated in a turbulence box actuated by a 10×10 synthetic jet array. Using LEDs and a single camera, free-surface flow measurements are carried out by Particle Image Velocimetry (PIV) simultaneously with Lagrangian tracking of the floaters, allowing the potential to characterise the coupling between the floater dynamics and the (sub)surface flow. Discrimination of the dispersed and continuous phases is carried out based on size. Individual floaters and clusters of floaters are successfully tracked throughout the field of view while they navigate through elongated and circular regions of high and low vorticity, characteristic features typically observed when a subsurface turbulent flow interacts with a free surface. Preliminary results of the floater-fluid interactions are presented to highlight the potential of this technique to better our understanding of floater-laden turbulent free surfaces.

1. Introduction

Dispersed two-phase flows at an air-water interface are prevalent in both natural and industrial settings. Examples include naturally occurring algal blooms in marine ecosystems and flotation processes in industry. In environmental ecosystems, turbulence at a free-surface may arise from wind-induced turbulence or the interaction of subsurface flow with the air-water interface. The presence of free-surface turbulence plays an important role in environmentally relevant flows that have societal implications such as the transport of floating microplastics or oil spills and regulation of gas absorption rates between the ocean and atmosphere (Herlina & Jirka (2008); Khakpour et al. (2011); D'Asaro (2014)).

In the situation of weak wind speeds, distinct free-surface features are dominated by imprints of coherent motions beneath the free-surface. Characteristic features like upwellings, boils, and scars

have been observed in free-surface flows where the surface remains relatively flat and unaffected by wind. Examples include, in experimental studies (open channel flow: Kumar et al. (1998)) and numerical simulations (open channel flow: Pan & Banerjee (1995); subsurface shear flow: Shen et al. (1999); subsurface homogeneous isotropic turbulence (HIT): Guo & Shen (2010)). For a more extensive review, the reader is referred to Sarpkaya (1996), Brocchini & Peregrine (2001) and Muraro et al. (2021). Experimental and numerical studies have utilised the characteristics of free-surface expressions to infer the subsurface flow characteristics (Tsai (1998); Savelsberg & van de Water (2006)) and the bedform (Mandel et al., 2019). In the current context, research on free-surface turbulence and its role in transporting microplastics or particles in general, holds practical significance particularly in predicting or optimising transport, and understanding fundamental turbulence-particle interaction.

Free-surface turbulence is garnering increased attention for its distinctive interactions with floating particles and the prevailing cluster dynamics. When subjected to a subsurface turbulent flow generated by an array of water sprinklers, floating particles initially distributed uniformly on the free-surface, have been observed to aggregate into string-like, high particle-density fronts (Cressman et al. (2004); Larkin et al. (2009)). Numerical simulations of particles dispersed over an open channel, have also reported particle clustering behaviour with fractal-like characteristics that have a lifetime longer than the turbulent structures in the flow (Lovecchio et al., 2013).

The underlying physical mechanism of clustering for particles confined to an air-water interface however, is profoundly different than for those suspended in a flow. The latter occurs as a result of particle inertia as they deviate from fluid trajectories (Eaton & Fessler, 1994). For floating particles on the other hand, buoyancy and interaction with surface features excited by the subsurface flow have been reported to drive the clustering. In particular, particles have been observed to flee upwelling regions that act like sources of fluid velocity and accumulate in downwelling regions that act like sinks of fluid velocity. Interestingly, Chor et al. (2018) reported that the buoyancy of a particle plays an important role in the characteristics of clusters formed for a given forcing condition. The importance of buoyancy of a particle is governed by the floatability parameter defined as $\beta = u'/u_T$ where u_T is the terminal velocity of a particle and u' is a typical fluid fluctuation (Chor et al., 2018). In addition to β, another commonly used parameter governing the particle behaviour is the Stokes number (St) which describes the ability of a particle to follow a typical fluid fluctuation. Both parameters imply an inherent relationship between the particle dynamics and the subsurface flow, an aspect that is still not well understood in particle-laden turbulent free surfaces.

Depending on the nature of the subsurface turbulent forcing, different dominating flow structures are expected to interact with the air-water interface, which in turn can affect the particle dynamics. A natural approach to study such societally relevant, complex dispersed two-phase flows would be to study elemental flows such as jets, shear layers or HIT interacting with a particle-laden free-surface. Experimental data on such flow systems however, remain scarce. In the current study, we

present an experimental method to simultaneously investigate the free-surface flow field and the behaviour of floating particles (hereafter termed as floaters) on the surface of a low-mean turbulent flow. The latter is produced in a turbulence box that drives a nearly homogeneous turbulent flow towards the free surface. Using LEDs and a single camera, measurements of the free-surface velocity field and the floater velocities are carried out using Particle Image Velocimetry (PIV) and Particle Tracking Velocimetry (PTV), respectively. We leverage the size difference between the dispersed and continuous phase to efficiently discriminate them. Implementation of a relatively simple Lagrangian tracking algorithm is enabled by the employment of monodisperse floaters. We demonstrate that we are successfully able to track floaters while simultaneously analysing the fluid flow in the vicinity of single floater and clusters of floaters. The findings of this study are anticipated to offer an experimental method to investigate dispersed two-phase flows at gas-liquid interfaces, and in particular, enable future work examining variable subsurface flow conditions and floater properties.

2. Experimental Setup

Experiments were performed in the TRACKqua facility of the Laboratory for Aero and Hydrodynamics at TU Delft. The facility shown in figure consists of a glass cuboidal tank of cross-section 1.2×1.2 m^2 and 1.4 m height. A water head of 1.2 m from the tank base is maintained during experiments. Turbulent forcing in the facility is generated by a pump array located at the base of the tank which directs fluid towards the free-surface. The array consists of 100 submersible pumps (Albin bilge pump 32 L/min at 12 V) placed in a 10×10 cartesian grid configuration with a spacing of 9.5 cm in both horizontal directions. Each pump produces a synthetic jet by drawing water radially from its base and ejecting it from the nozzle located at about 19 cm from the pump base. 3D printed 90° elbows with a nozzle diameter of 14 mm and a length of approximately $7.5\ d$ (d being the nozzle diameter) were connected to the pumps. This was done to provide the flow enough length to straighten out and overcome any secondary swirling effects due to the elbow. The pumps are controlled by an ethernet based solid state relay (ETH8020 by Devantech). When triggered, each relay closes a circuit supplying 12 V at 1.8 Amps to a specific pump.

The pattern of actuation of the pumps is carried out using a random spatio-temporal algorithm known as the Sunbathing algorithm (Variano & Cowen, 2008), which has been shown to closely approximate zero-mean-flow HIT at relatively high Reynolds numbers compared to other algorithms (Pérez-Alvarado et al., 2016). Individual jets are turned on and off, with duration of the periods chosen from a Gaussian distribution described by their mean and standard deviation (μ_{on}, μ_{off} and σ_{on}, σ_{off} respectively). μ_{on} and μ_{off} are related through the source fraction ϕ ($\phi = \mu_{on}/(\mu_{on} + \mu_{off})$), defined as the average fraction of jets firing at any instant of time. ϕ plays an important role in controlling the momentum input to the flow and hence the turbulence intensity, with values of $\phi \approx 10 - 20$ % found to be optimal in maximising the turbulent fluctuations relative to the mean

flow (Variano & Cowen, 2008). In the current study, we perform measurements with $\mu_{on} = 0.7$ s, $\phi = 40$ % as the actuation parameters. Preliminary experiments indicated that under conditions of relatively high μ_{on} and low ϕ levels (for instance, $\mu_{on} = 3$ s; $\phi = 12.5$ %), the flow qualitatively exhibited poor mixing with discernible jet imprints observed at the free-surface. Using a similar random-jet-stirred turbulence forcing, Bang & Pujara (2023) highlighted the important role of μ_{on} in mixing of individual jets with background turbulence. They found signatures of individual jets overpowering the background turbulence for increasing μ_{on} which prevents the former from becoming fully mixed. Within the framework of our current study centered on a lightly-deformed free-surface regime (Froude number $(Fr) \approx \mathcal{O}(10^{-3})$ and Weber number $(We) \approx \mathcal{O}(10^{-2})$) and minimal wave generation, it was deemed necessary to employ a low value for μ_{on}.

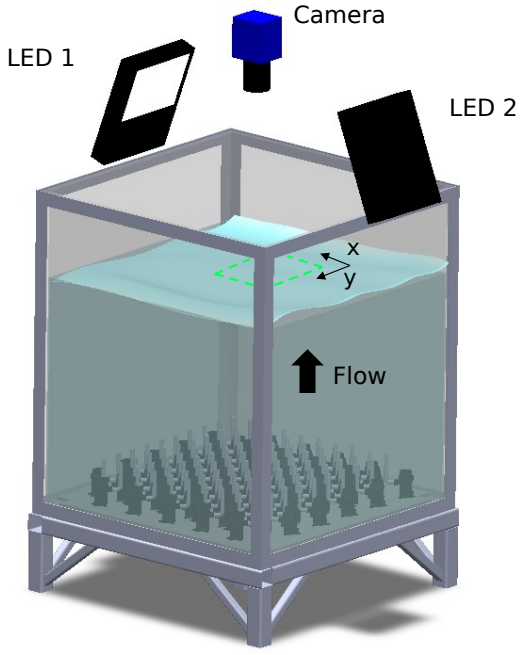

Figure 1. A model of the experimental facility TRACKqua with a pump array located at the base of the tank which drives turbulence towards the free surface. The green dotted rectangle represents the field of view captured (17×20 cm^2 in x and y directions respectively).

Simultaneous measurements of the free-surface flow field and floaters are done using a single-camera planar PIV setup. The flow was seeded with Polyamide particles that have a mean diameter of 60 μm and a specific gravity ≈ 1. Monodisperse polypropylene spheres of diameter 2 mm (d_p) and specific gravity $\rho_p/\rho = 0.87$ were used as the dispersed phase (ρ_p and ρ being the density of the floaters and fluid respectively). The volume of submergence of the floaters in water were found to range between 88 % and 92 %. Relevant dimensionless parameters for the dispersed phase in the current study are $d_p/\mathcal{L} \approx 0.06$, $d_p/\eta \approx 1.6$, $St_\eta \approx 10^{-1}$ and $\beta \approx 10^{-2}$, where $\mathcal{L}$ and

η are the integral length and Kolmogorov scales of the single-phase flow, respectively. A single camera (LaVision Imager sCMOS) mounted with a Nikon objective of focal length 35 mm, images the free-surface at the centre of the tank capturing an area of approximately 17×20 cm^2 at a resolution of 12.5 pix/mm. Two continuous LED lights (Noxion LED Floodlight 170 Watts) were used to illuminate the free-surface from above. The aperture of the camera was opened completely ($f_{\#} = 1.8$) to minimise the focal depth (≈ 1.3 mm) and prevent imaging of any fluid tracers *below* the free-surface. As a consequence of a low Fr utilised in the study, any unwanted light reflections from the undulations of the free-surface were minimised. A frame rate of 8 Hz was used to obtain a time-resolved data set. Considering the difference in size and number density of the tracers and floaters, dedicated processing techniques are used to obtain simultaneous velocity fields of the tracers and floaters (PIV and PTV, respectively).

In what follows, velocity vectors of the fluid and floaters are represented by V_f and V_p respectively, with the corresponding components in the x and y directions being (u_f, v_f) and (u_p,v_p) respectively.

3. Phase discrimination

Discrimination between the dispersed and continuous is carried out by leveraging the high ratio between the floater size and the fluid tracer size ($\mathcal{O}(10^2)$). A median filter is first used to remove noise followed by a binarization to separate high intensity regions from the background. The boundaries of high intensity regions (see 'Identify boundaries' in figure 2 (in green)) are traced using Matlab's in-built Moore-Neighbour tracing algorithm. A PDF of the areas enclosed within the detected boundaries exhibits multiple peaks (see figure 2). These peaks, indicating floater clusters of different sizes, are then separated according to the number of floaters. The spread in distribution of areas observed for one, two and three floaters (red, blue and green in pdf of figure 2), stems as an artifact of imaging. Inhomogeneous illumination or halos present around floaters, can contribute to the spread in the distribution observed. The boundaries identified are then subsequently utilized as a mask in the raw images to extract the floaters through inversion (see figure 3). To isolate the flow tracers, the masks are first enlarged by morphological dilation to remove any halos present around the floaters.

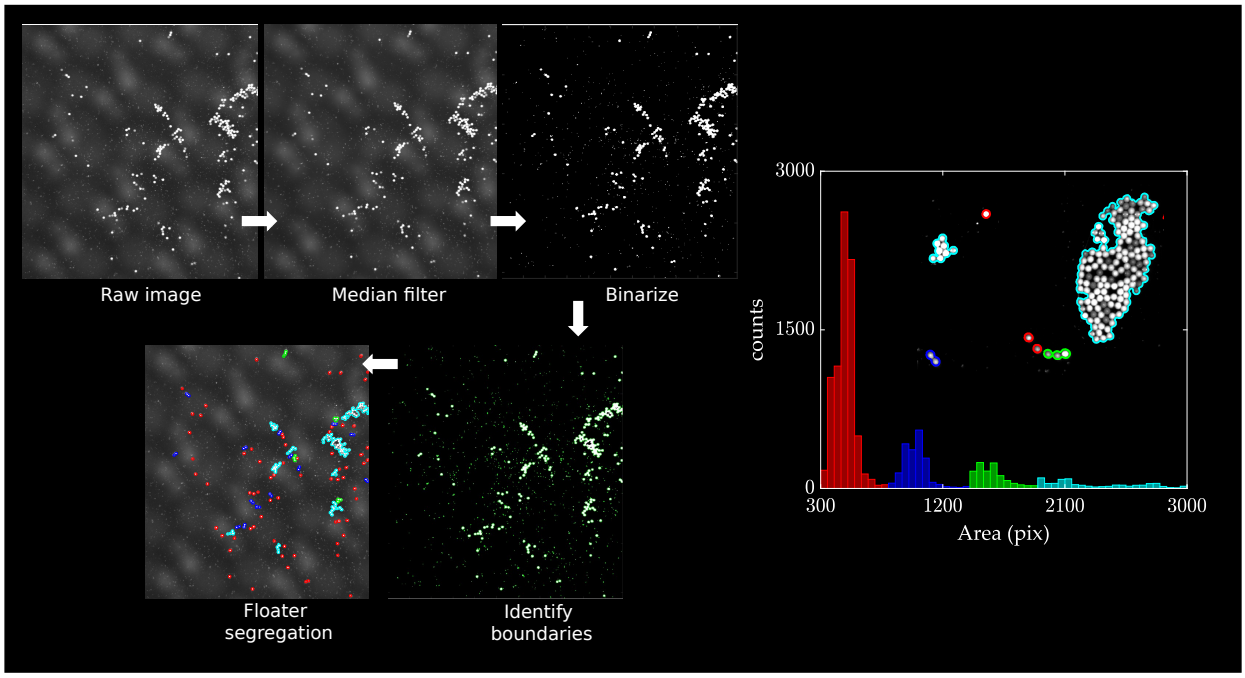

Figure 2. Process of discrimination between the continuous and dispersed phases. Also shown is a PDF of areas (pix) enclosed within the boundaries detected allowing for a segregation based on the number of floaters within a boundary (in different colours).

The "holes" left by the masks in the raw image containing the position of the floaters, are filled with noise with an amplitude comparable to the background noise of the raw image. This process (see figure 3) is carried out on the whole image set. Using the discriminated phases (see figure 4), velocity fields of the free-surface and floaters are then obtained using planar PIV and PTV respectively.

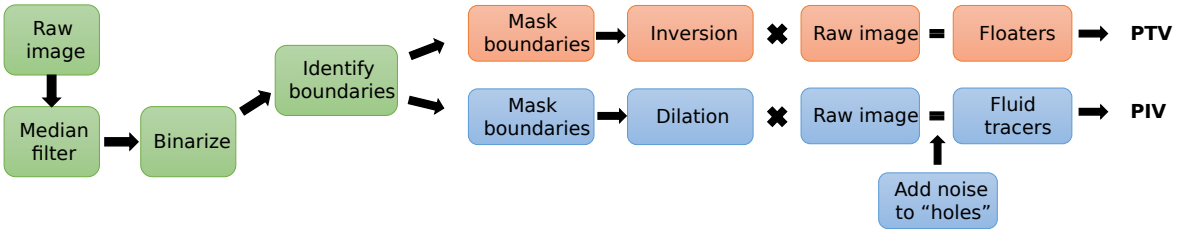

Figure 3. A summary of steps involved in the phase discrimination.

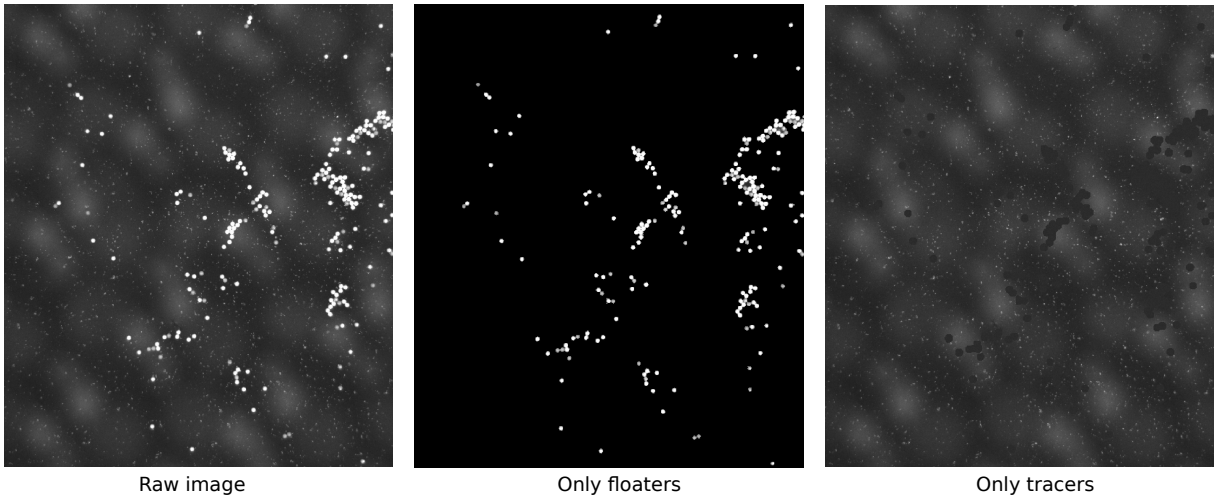

Figure 4. A Raw image separated to an only floaters and an only flow tracers image.

4. Velocity estimation

4.1. Particle Image Velocimetry

Single-phase PIV processing (flow only) and the segmented tracer-only two-phase images were processed using Davis 10.2.1. A final interrogation window size of 64×64 pix with 75% overlap was employed resulting in a vector spacing of 1.28 mm $\approx \eta$ (Kolmogorov length scale), for the current flow conditions (see table 1). The relatively high overlap was selected to improve sampling in regions of high velocity gradients (Tokgoz et al., 2012). Vector validation was carried out using the universal median test to remove any spurious vectors (Westerweel & Scarano, 2005).

Table 1. Statistics of the single phase free-surface flow conditions measured using PIV.

Mean flow strength	$M = \overline{u}/u'$ [%]	15.7
Longitudinal Integral length scale	$\mathcal{L}_{11}$ [mm]	31.2
Transverse Integral length scale	$\mathcal{L}_{22}$ [mm]	35.1
Anisotropy	$\mathcal{L}_{11}/\mathcal{L}_{22}$	0.9
Velocity fluctuation rms (in x)	u'_{rms} [mm/s]	3.1
Velocity fluctuation rms (in y)	v'_{rms} [mm/s]	3.5
Kolmogorov length scale	η [mm]	1.3
Kolmogorov velocity scale	u_η [mm/s]	0.81
Dissipation rate	ϵ [mm^2/s^3]	0.42
Taylor micro scale	λ [mm]	17.8
Taylor Reynolds number	Re_λ	51

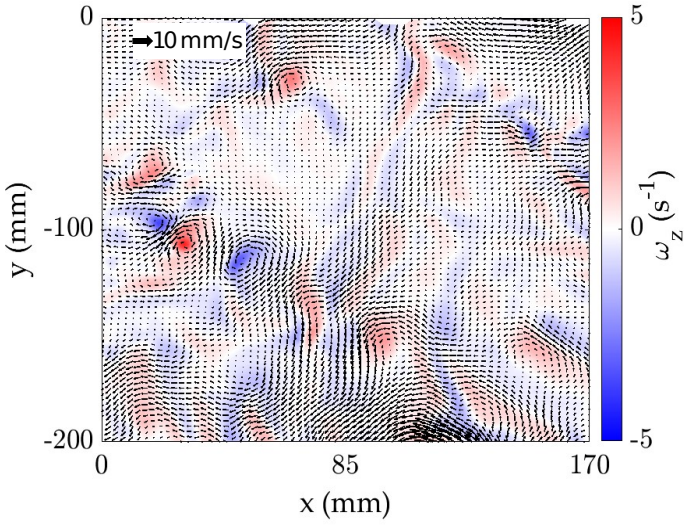

Figure 5. An example of an instantaneous single-phase flow field using PIV superimposed on the corresponding vorticity field ω_z.

A total of 3900 independent image pairs were used to estimate the statistics reported in table 1. Velocity fluctuations are computed by subtracting the instantaneous spatial means from the instantaneous velocity fields. The mean flow strength, which compares the magnitude of mean flow relative to turbulent fluctuations is observed to be about 16 %. Here, we calculate the mean flow strength using the absolute values of the mean velocities to avoid excessive minimisation of the former by spatial averaging. The integral length scales, $\mathcal{L}_{11}$ and $\mathcal{L}_{22}$ are estimated using the two-point autocorrelation function, and are observed to be of the same order of the nozzle diameter (d), with a slight anisotropy between the longitudinal and transverse directions. A direct comparison of the single-phase characteristics in the current study with studies in literature using a similar turbulent forcing however, is not possible. While the latter report statistics of the bulk turbulent flow (for example Variano & Cowen (2008)), the current study focuses on the characteristics of the free-surface flow. Future experiments are planned to measure the bulk turbulence properties.

A representative single-phase instantaneous free-surface vorticity field is shown in figure 5. Qualitatively speaking, the vorticity field exhibits a plethora of topological features at the free surface. Elongated regions exhibiting both positive and negative vorticity, along with approximately circular areas of heightened vorticity are found scattered across the free-surface. These surface features observed are characteristic of the interaction between a subsurface turbulent flow and a free surface (Shen et al. (1999); Yang & Shen (2011)), and are anticipated to influence the behavior and transport of the floaters. A further characterisation of the single-phase flow is beyond the scope of the current work, and will be addressed in a future study.

4.2. Particle Tracking Velocimetry

Floaters in the segmented two-phase images are identified using Matlab's in-built Circular Hough transform algorithm that identifies circles in an image. Occasionally, false positives occur: overlapping circles when multiple floaters are clustered or centroids of circles identified at the edge of floaters due to uneven illumination of the latter. False positives are eliminated by verifying that the identified centroids are within high-intensity regions, and then applying a minimum distance threshold between centroids equivalent to a floater diameter.

At time t, all floaters are first identified. To estimate their displacement at time $t + dt$, a circular search radius corresponding to the maximum expected displacement ($r_s \approx 2d_p$) is used. All floaters found within that radius at time $t + dt$ are then assumed as possible matches. For all of them, a refined search, using an elliptical search area, is made for time $t + 2dt$. The ellipse is aligned with each floater's displacement vector dx_p from the previous time-step (t to $t + dt$), its major axis corresponding to $|dx_p|$ and its minor axis to d_p. An elliptical search radius proved useful when displacements exceeded d_p and in reducing potential number of matches. Finally, the best trajectory is kept when the algorithm can match the floater to its nearest neighbour (if there is one), in addition to minimizing the angle between the two displacement vectors (t-$t+dt$ and $t+dt$-$t+2dt$). This criterion is imposed to prevent false positives (if any) and was found to be effective for well-time resolved data. This procedure is followed for subsequent time-steps, $t + 3dt, t + 4dt$ and so on.

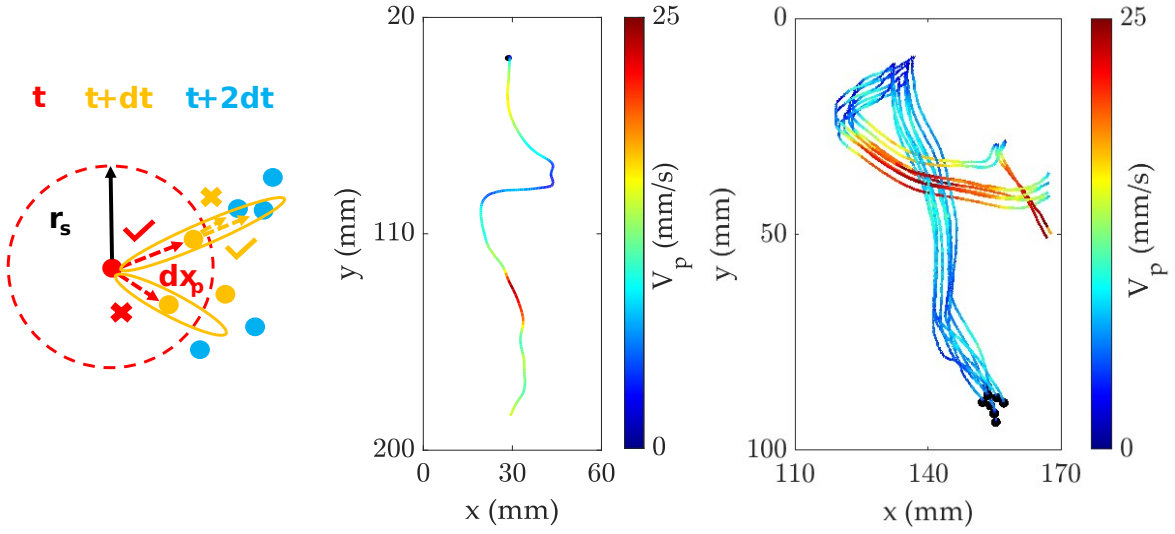

Figure 6. Left: A schematic of the PTV algorithm. Right: Sample trajectories of an individual floater and a cluster of floaters with tracks coloured by the magnitude of the instantaneous floater velocities. The initial position of floaters is marked by black filled circles.

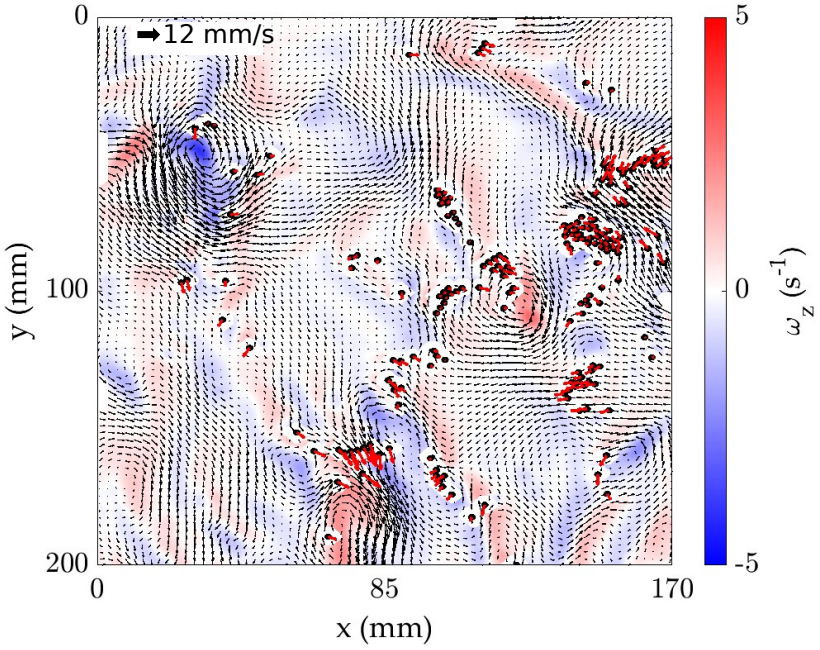

Figure 7. An example of a combined instantaneous PIV/PTV field superimposed on the corresponding vorticity field ω_z. The fluid phase is represented by thin black arrows. The dispersed phase is represented by black filled circles and red velocity vectors.

Occasionally, a floater might go undetected in a frame. In such cases, the trajectory of the floater is terminated when no match is found and is restarted when the same floater is detected in a subsequent frame. Sample tracks of an isolated floater and clustered floaters coloured by instantaneous floater velocities are shown in figure 6. The algorithm is successfully able to capture the path taken by a floater as they navigate through different regions of the flow. Particularly, the acceleration and deceleration phases of the floaters appear to be well-correlated with the curvature of the path. Besides individual tracks, the collective motion within a cluster is also effectively captured (see right panel of figure 6). Individual floaters within the cluster appear to experience similar phases of acceleration and deceleration as the cluster traverses different flow regions. Analyzing the free-surface flow field around clustered floaters alongside the motion of floaters within a cluster can aid in predicting the formation, evolution, and disintegration of these clusters.

5. Preliminary Results

A typical instantaneous combined PIV/PTV field superimposed with the corresponding vorticity field (ω_z) is shown in figure 7. The fluid velocities are represented by thin black arrows while the floaters are represented by black filled circles with red velocity vectors. In this section, we leverage the simultaneous fluid/floater measurements to preliminary discuss some velocity characteristics

of the dispersed and continuous phases. Simultaneous measurements of the dispersed and continuous phases are exploited first to analyze statistics of instantaneous floater velocities compared to the single-phase and two-phase instantaneous flow velocities (see figure 8). The single-phase and two-phase velocities are normalised by their respective rms velocity fluctuations while the floater velocities are normalised by the rms velocity fluctuation of the two-phase flow. The two-phase flow appears to be mostly unaffected by the dispersed phase. Floater velocities on the other hand, exhibit strong tails with cases of floaters reaching almost $4-5$ times the fluid velocity fluctuations.

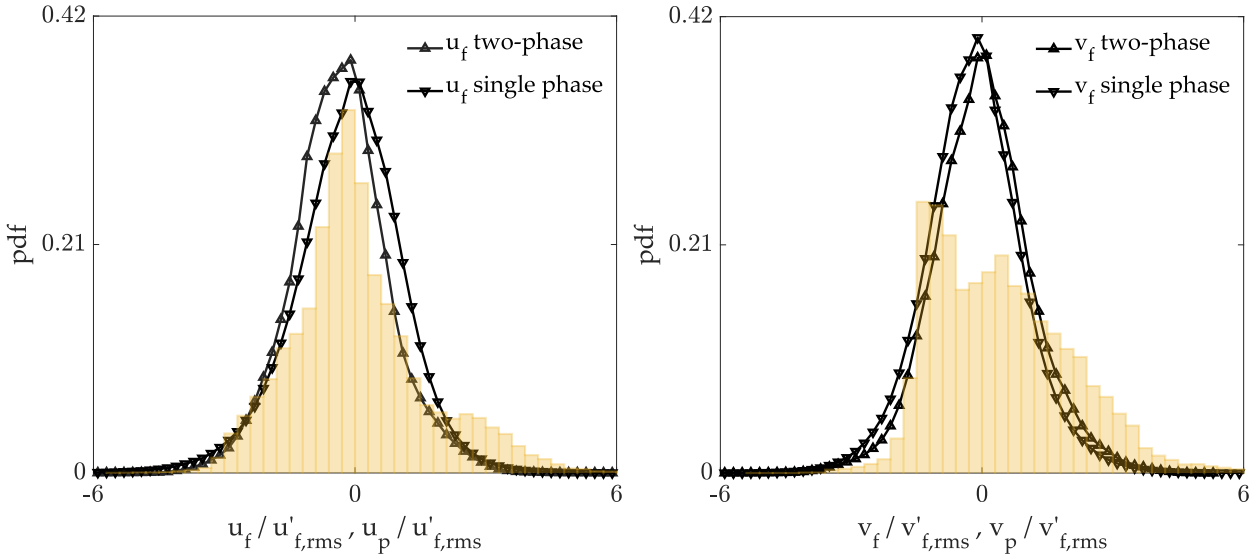

Figure 8. PDF of instantaneous velocities of all floaters in x and y directions (u_p and v_p respectively) normalised by rms velocity fluctuation of the two-phase flow (bar plot). Also shown is PDF of instantaneous single phase (black downward pointing triangles) and two-phase (black upward pointing triangles) flow velocities normalised by their respective rms velocity fluctuations.

To identify the contribution of isolated floaters to this PDF, we identify floaters that are not part of a cluster (red coloured distribution in the PDF of figure 2). Floaters are considered isolated regardless of whether they were previously part of a cluster or will join one in the future. For lack of a better definition in literature, we define clusters as two or more floaters in the current study. Figure 9 shows the instantaneous velocities of isolated floaters compared to the single-phase and two-phase instantaneous flow velocities. The distribution of velocities of isolated floaters appear to be relatively Gaussian. While there is no noticeable change in the spread of the distribution for u_p compared to figure 8, v_p of the isolated floaters appear to be relatively less intermittent.

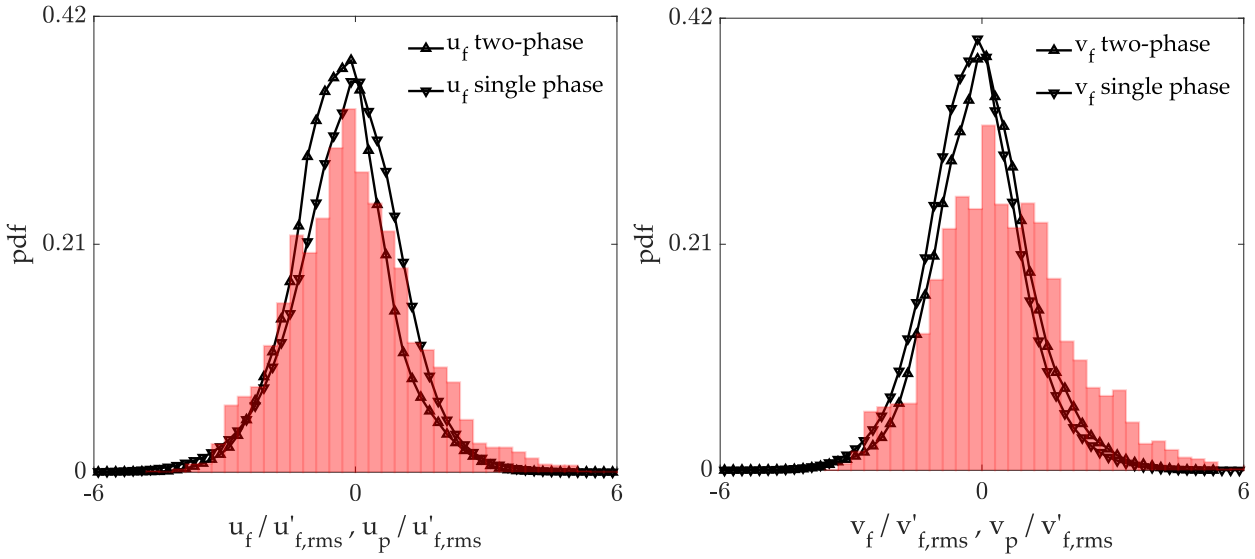

Figure 9. PDF of instantaneous velocities of isolated floaters (see red distribution in figure 2) in x and y directions (u_p and v_p respectively) normalised by rms velocity fluctuation of the two-phase flow (bar plot). Also shown is PDF of instantaneous single phase (black downward pointing triangles) and two-phase (black upward pointing triangles) flow velocities normalised by their respective rms velocity fluctuations.

To further analyze the intermittency of floaters with respect to the flow, future work is planned to correlate instances of these extreme events to the surrounding flow both spatially and temporally. High floater accelerations can lead to finite relative velocities or slip between the particles and the flow, which can potentially have a feedback effect on the flow. While a systematic variation of physical parameters (d_p, flow and floater Reynolds number (Re_λ and Re_p respectively), area fraction of the floaters (ϕ), buoyancy of a floater (in terms of β) to name a few) is needed to isolate the different mechanisms at play, the current experimental technique illustrates the potential to do so.

6. Conclusions

In this study, we present an experimental method to measure dispersed two-phase flows at gas-liquid interfaces. We demonstrate the applicability of this technique in studying a lightly-deformed turbulent free-surface laden with spherical floating particles (or floaters). A relatively simple setup is used to track floaters while simultaneously analyzing the fluid flow around both individual floaters and clusters of floaters. We demonstrate that we are able to successfully track individual and clustered floaters throughout the field of view. Using Lagrangian statistics of floaters such as floater velocity and acceleration supported by simultaneous Eulerian flow field measurements, can aid in predicting the formation and destruction of clusters. Future experimental campaigns are planned to vary the parameter space to further understand floater-turbulence interactions. We

anticipate the applicability of this technique to simultaneously analyze the dispersed and continuous phases at air-water interfaces to enhance our understanding of floater-laden turbulent free-surfaces, a topic that still remains largely unexplored in literature.

Acknowledgements

The authors would like to gratefully acknowledge the help of the DEMO team (Martijn Karsten, Daniel van Baarle), Bart Hoek, Jan Graafland, Jasper Ruijgrok, Edwin Overmars and Gertjan Mulder during various stages of the experimental campaign.

References

Bang, J. Y., & Pujara, N. (2023). Homogeneous turbulence in a random-jet-stirred tank. *Experiments in Fluids*, *64*(185), 1-22.

Brocchini, M., & Peregrine, G. H. (2001). The dynamics of strong turbulence at free surfaces. Part 1: Description. *J. Fluid Mech*, *449*, 225-254.

Chor, T., Yang, D., Meneveau, C., & Chamecki, M. (2018). Preferential concentration of non-inertial buoyant particles in the ocean mixed layer under free convection. *Physical Review Fluids*, *3*(064501), 1-18.

Cressman, J. R., Davoudi, J., Goldburg, W. I., & Schumacher, J. (2004). Eulerian and Lagrangian studies in surface flow turbulence. *New Journal of Physics*, *6*(53), 1-25.

D'Asaro, E. A. (2014). Turbulence in the Upper-Ocean mixed layer. *Annu. Rev. Mar. Sci.*, *6*, 101-115.

Eaton, J. K., & Fessler, J. R. (1994). Preferential concentration of particles by turbulence. *Int. J. Multiphase Flow*, *20*, 169-209.

Guo, X., & Shen, L. (2010). Interaction of a deformable free surface with statistically steady homogeneous turbulence. *J. Fluid Mech*, *658*, 33-62.

Herlina, & Jirka, G. H. (2008). Experiments on gas transfer at the air–water interface induced by oscillating grid turbulence. *J. Fluid Mech*, *594*, 183–208.

Khakpour, H. R., Shen, L., & Yue, D. K. P. (2011). Transport of passive scalar in turbulent shear flow under a clean or surfactant-contaminated free surface. *J. Fluid Mech*, *670*, 527–557.

Kumar, S., Gupta, R., & Banerjee, S. (1998). An experimental investigation of the characteristics of free-surface turbulence in channel flow. *Physics of Fluids*, *10*, 437-456.

Larkin, J., Bandi, M. M., Pumir, A., & Goldburg, W. I. (2009). Power-law distributions of particle concentration in free-surface flows. *Physical Review E*, *80*(066301), 1-5.

Lovecchio, S., Marchioli, C., & Soldati, A. (2013). Time persistence of floating-particle clusters in free-surface turbulence. *Physical Review E*, *88*(033003), 1-6.

Mandel, T. L., Gakhar, S., Chung, H., Rosenzweig, I., & Koseff, J. (2019). On the surface expression of a canopy-generated shear instability. *J. Fluid Mech*, *867*, 633-660.

Muraro, F., Dolcetti, G., Nichols, A., Tait, S. J., & Horoshenkov, K. V. (2021). Free-surface behaviour of shallow turbulent flows. *Journal of Hydraulic Research*, *59*, 1-20.

Pan, Y., & Banerjee, S. (1995). A numerical study of free-surface turbulence in channel flow. *Physics of Fluids*, *7*, 1649-1664.

Pérez-Alvarado, A., Mydlarski, L., & S., G. (2016). Effect of the driving algorithm on the turbulence generated by a random jet array. *Experiments in Fluids*, *57*, 1-15.

Sarpkaya, T. (1996). Vorticity, free surface, and Surfactants. *Annu. Rev. Fluid. Mech*, *28*, 83-128.

Savelsberg, R., & van de Water, W. (2006). Experiments on free-surface turbulence. *J. Fluid Mech*, *619*, 95–125.

Shen, L., Zhang, X., Yue, D. K. P., & Triantafyllou, G. S. (1999). The surface layer for free-surface turbulent flows. *J. Fluid Mech*, *386*, 167-212.

Tokgoz, S., Elsinga, G. E., Delfos, R., & Westerweel, J. (2012). Spatial resolution and dissipation rate estimation in Taylor–Couette flow for tomographic PIV. *Experiments in Fluids*, *53*, 561–583.

Tsai, W.-T. (1998). A numerical study of the evolution and structure of a turbulent shear layer under a free surface. *J. Fluid Mech*, *354*, 239-276.

Variano, E. A., & Cowen, E. A. (2008). A random-jet-stirred turbulence tank. *J. Fluid Mech*, *604*, 1-32.

Westerweel, J., & Scarano, F. (2005). Universal outlier detection for PIV data. *Experiments in Fluids*, *39*(6), 1096-1100.

Yang, D., & Shen, L. (2011). Simulation of viscous flows with undulatory boundaries. Part 1: Basic solver. *Journal of Computational Physics*, *230*, 5488-5509.